DESIGN AND EXPERIMENTAL RESEARCH ON THE COMBINED FLASH-BINARY GEOTHERMAL POWER GENERATION SYSTEM DRIVEN BY LOW-MEDIUM TEMPERATURE GEOTHERMAL SYSTEM

by

Chao LUO [a,b,c,d*], ***Jun ZHAO*** [b], ***Yongzhen WANG*** [b], ***Hongmei YIN*** [b], ***Qingsong AN*** [b], ***and Yulie GONG*** [b,c,d]

[a] School of Architecture and Civil Engineering, Huizhou University, Huizhou, Guangdong, China
[b] Key Laboratory of Efficient Utilization of Low and Medium Grade Energy, Tianjin University, Ministry of Education, Tianjin, China
[c] Key Laboratory of Renewable Energy, Chinese Academy of Sciences, Guangzhou, Guangdong, China
[d] Guangdong Provincial Key Laboratory of New and Renewable Energy Research and Development, Guangzhou, Guangdong, China

Original scientific paper
https://doi.org/10.2298/TSCI181112013L

To match for the different temperature of the geothermal resource and strengthen the flexibility of organic Rankine cycle, a variable capacity power generation superstructure based on flash and organic Rankine cycle for geothermal energy was proposed. A combined flash-binary experimental prototype is newly established to investigate thermodynamic performance both on system and equipment in this paper. Pressured hot water is adopted as the extensive worldwide existed hydrothermal geothermal resource, eliminating the influence of the used heat transfer oil on evaporating process. The experimental results show that there is an optimal mass-flow rate of R245fa under the condition of different heat source temperature. Flash and binary power subsystem dominate the flash-binary power system, respectively, when the heat source temperature is 120 ℃ and 130 ℃. The isotropic efficiency of modified compressor just between 0.2 and 0.25. The power output of per ton geofluid are 0.78 kWh/t and 1.31 kWh/t, respectively, when the heat source temperature are 120 ℃ and 130 ℃. These results will predict the operation data of flash-binary power plant driven by the low-medium temperature geothermal water for construction in western of China.

Key words: *geothermal power plant, flash system, organic Rankine cycle, experiment, exergy, efficiency*

Introduction

Renewable energy resources are environment-friendly and inexhaustible. The renewable energy power generation systems are growing very fast worldwide either in the developing or developed regions. Despite lots of distinct advantages of power generation systems based on renewable resource, they suffer apparent disadvantages, such as dependency on climate, complex configurations and high investment of conversion. Therefore, in order to meet the

* Corresponding author, e-mail: huangle@hzu.edu.cn

increasing world-wide demand for electricity, an urgent need of efficient and reliable renewable power generation at low cost is intensely observed worldwide.

Geothermal power generation has been proved as one of the most promising renewable energy power generation technologies for its consecutiveness and stabilization [1]. In other words, the feasibility of geothermal power plants is determined by environment cleanliness, economic efficiency, and the highest indicators of installed capacity utilization (among RES) [2]. Figure 1 displays the capacity and the number of units for each type of geothermal power plants in the world 2015 [3].

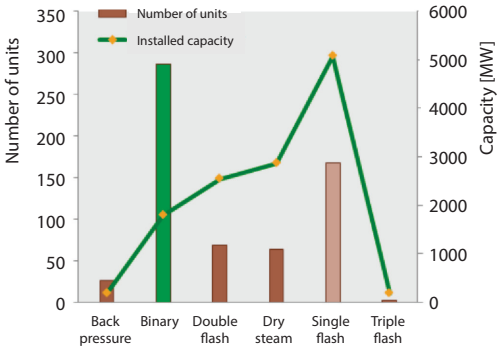

Figure 1. Installed capacity and number for each geothermal plant typology in the world

In fact, many countries are rich in geothermal resource such as Iceland, New Zealand, Indonesia, Kenya, America, and China, ranging from the shallow ground to the hot dry rock, and down even to the molten rock which called magma in the earth [4]. However, the low and medium temperature hydrothermal geothermal resource below 150 ℃ will play a significant role in the view of technical and economic conditions of future decades in the western of China. Flash system is the most common power technology of geothermal power plant because of the stability and convenience. The organic Rankine cycle (ORC) is also the potential technology for its excellent efficiency and flexible lay-out driven by the low and medium heat source [5, 6].

The performance of a geothermal flash power system is analyzed from the view of thermodynamic, exergy and exergoeconomic [7-9]. Scaling and condenser temperature as constrained conditions are discussed in the double-flash geothermal power plants [10]. At present, the focus on geothermal power plant is to improve performance or modified the existing flash power plants [11]. The ORC is the typical representative of the geothermal binary power system. The ORC have been investigated on its working fluid screening [12, 13], performance optimization [14, 15] and dynamic simulation [16, 17] in the past several decades. Meanwhile, medium-large-scale ORC prototypes and engineering cases have been carried out [18-21]. However, the expensive design and manufacture costs of expander imposes the largest restriction on commercial application of the small-scale ORC system, investment is much larger than 1500 $ per kW. The smaller capacity is, the investment increases larger. Obviously, ORC will not only be used in geothermal energy but also applied to many types of hot source extensively, if the cost of expander can be lower. Fortunately, replacing expander with a modified reversed compressor in ORC gives researchers a feasible way [22, 23], and a great many air-conditioning enterprises have tried to enter into ORC market. The most types of small scale ORC expanders modified from compressor is scroll type, Chang *et al.* [24] experimentally investigated an ORC with a scroll expander. The maximal shaft power output and electricity power output were 1.74 kW and 1.375 kW when using R245fa as working fluid, respectively. Bracco *et al.* [25] also investigated an ORC system with a scroll expander, the system output power was 1.1~1.5 kW when pressure ratio of working fluid of R245fa was 5~6.5. Quoilin *et al.* [26] investigated an ORC prototype with an open-drive oil-free scroll expander and used R123. The maximal isentropic efficiency of the expander was 68%. Twomey *et al.* [27] reported on a small-scale ORC using R134a and a scroll expander. The results demonstrated a maximal isentropic efficiency of the expander of 59% with a corresponding ORC efficiency of 3.47%. Liu *et al.* [28] obtained the

highest isentropic efficiency of the expanders modified from scroll compressor distributed in the range of 57~84.9%.

The flash-binary power system, which combines the benefits associated with both flash cycles and binary cycles, have been investigated by several researchers recently for the better exploitation of high temperature geothermal resources. Zeyghami [29] gives the performance analysis and binary working fluid selection of the flash-binary geothermal system; many working fluids can be selected when the geothermal temperature ranges from 150-250 °C based on the performance of the power system. Besides thermodynamic analysis, exergy cost evaluation and exergoeconomic analysis are also studied [30-33], First law efficiency, exergy efficiency, exergy cost and power cost are calculated based on the self-built physical model by numerical simulation method.

The optimal design of geothermal flash or binary power plants is studies in University of Pisa and Stanford University. The University of Tabriz in Iran and University of Gaziantep in Turkey focus on exergoeconomic analysis of flash-binary power system. Berlin geothermal power plant added a binary power system based on original flash power system by LaGEO in El Salvador. In China, experiment and simulation are studied by Tianjin University, Xi'an Jiaotong University and Chinese Academy Science.

It can be seen that there is no experimental data for the flash-binary power system. However, the overwhelming majority of ORC preliminary investigation used conduction oil as the intermediate heat transfer medium of hot source, neglecting the influence of the vast difference of the heat transfer property between geothermal hot water and conduction oil on the ORC system performance. In fact, excepting the thermodynamic parameters, the heat transfer medium character also affects the dynamic response of the flash-binary system. Therefore, this paper explores the steady performance with working fluid of R245fa in different mass-flow rates, and dynamic response of the flash-binary system under the condition of varying heat source temperature. It is noted that, hot water of 120 °C and 130 °C are adapted to simulate the low and medium temperature hydrothermal geothermal resource without using an intermediate heat transfer medium. Scroll expander reversed from an air-conditioning compressor is employed and the system is tested.

Experimental set-up and procedure

The schematic diagram and experiment photograph of flash-binary power system are shown in figs. 2 and 3. The total capacity of the power system is 2 kW. The primary design data of the experiment test are shown in tab. 1.

Table. 1 Basic design data of the experiment test

Heat source temperature [°C]	Cooling water temperature [°C]	Preheater area [m^2]	Evaporator area [m^2]	Condenser area of ORC [m^2]	Condenser area of flash [m^2]
120	28	0.34	5.88	2.88	5

Experimental set-up

The experimental test of flash-binary power system is composed of electric pressurized water boiler, flash power subsystem, binary power subsystem and cooling tower. An electric pressurized water boiler (AEWT/H-30-80) is simulated as the geothermal water, with four electrical heating rods having a capacity of 80 kW. The cooling tower (DBNL-15T) is installed

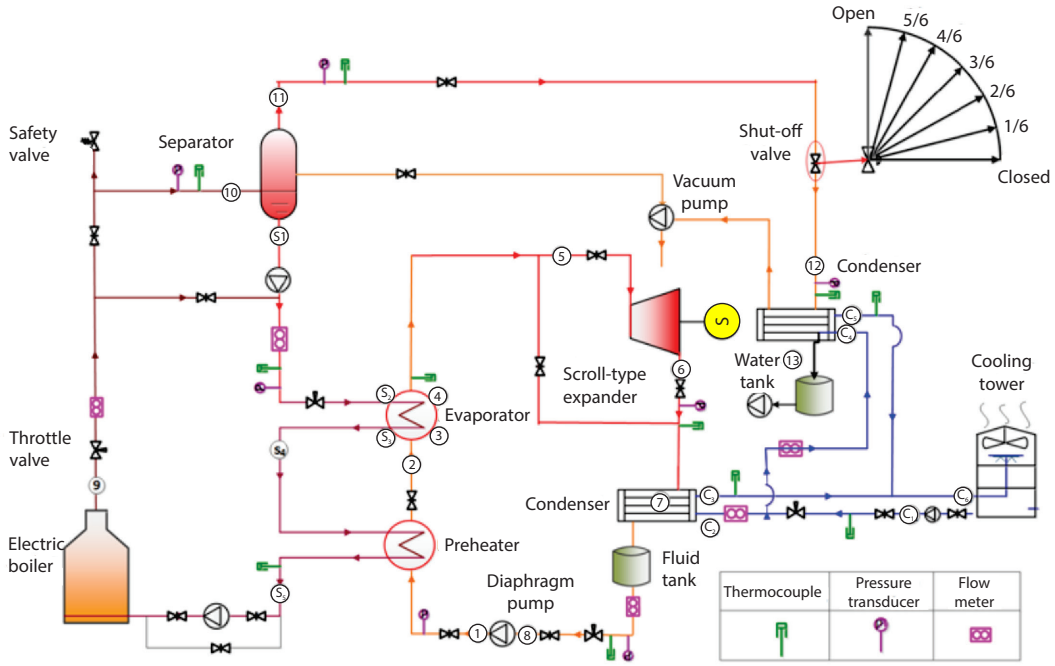

Figure 2. Schematic diagram of flash-binary system

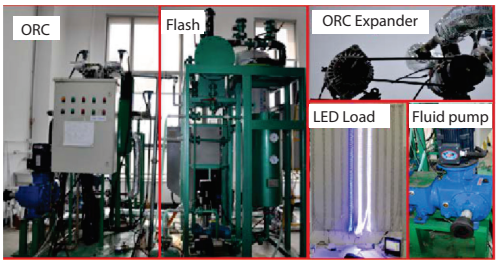

Figure 3. Photographs of flash-binary system test

at outdoor, extracting heat from condenser to air environment. For power generation system, an efficient expander with low power capacity is not available in the market. Hence, a modified compressor for reverse direction installation is used to simulate the expansion in the binary power subsystem, and a shut-off valve for controlling opening fraction is used to simulate the expansion in the flash power system.

Flash power subsystem is composed of five major components: a throttle valve, a flashing separator, a vacuum pump, a shut-off valve and a condenser. The shut-off valve is used to simulate the expansion in the flash power subsystem by controlling the opening fraction of the valve. The vacuum pump is used to pump gas in the condenser and the flashing separator.

Binary power subsystem includes a diaphragm pump, a preheater, an evaporator, a scroll-type expander and a condenser. The working fluid mass-flow rate is controlled by the diaphragm pump (SJ3-M-630/1.5) with different values. The preheater, evaporator and condenser are plate heat exchangers, and the insulating foam is equipped around them to avoid the heat loss. The scroll-type expander is modified from a small auto air-conditioning compressor (ATC-066-J10) with a volume ratio of about 4.65. The expander shaft power is transferred to the direct current permanent magnet motor (JFZ168-H) by pulley and belt. Then, the direct current produced and it is consumed by the LED lamp. The R245fa is used in our study as the working fluid due to its excellent environmental property and better thermodynamic performance, especially its good match ability at low and medium temperature heat source.

The simulated high temperature geothermal water from electric pressurized water boiler is partially vaporized by a throttle valve, and then enters to flashing separator. The saturated steam and water are separated in the separator. The separated saturated steam enters to the shut-off valve in flash power subsystem for reducing pressure and the separated saturated water enters to evaporator for heating R245fa in binary power subsystem. The separated saturated steam is cooled in the condenser by the cooling water. The separated saturated water flows into evaporator, preheater and finally into the boiler. The condenser working fluid of R245fa is pumped to preheater by diaphragm pump. The R245fa is heated to saturated liquid by separated water in preheater. The superheated vapor of R245fa from evaporator enters to expander to generate electricity, and then cooling in the condenser by cooling water. The working fluid finished a closed cycle in condenser, preheater and evaporator.

Experimental procedure and measurement

The flash-binary power experiment test includes lots of equipment and measuring instruments. Experiment must be operated carefully. The experimental procedures are as follows:

- the system is started with cooling water circulation in the condenser of flash and binary subsystem,
- switch on the electric pressurized water boiler to heat the water and open the vacuum pump of flash power subsystem; make sure the flash power subsystem operates stably by adjusting hot water valve to ensure the water level at 1/3 height of the separator,
- open the working fluid diaphragm pump of binary power subsystem, and make the modified expender rotate when the R245fa vapor at outlet of evaporator is at super heat state,
- change the mass-flow rate of R245fa and record the experiment operation data; reset the boiler temperature from 120 °C to 130 °C and repeat the steps from (1) to (4), and

The temperature and pressure in the main components are measured by PT100 and pressure transducers, respectively. The R245fa and water mass-flow rate measured by Coriolis flowmeter and electromagnetic-flowmeter, respectively. Various operating parameters such as pressure, temperature, and flow rates are monitored.

Data acquisition and processing

The fraction of shut-off valve is 1/6 in flash power subsystem and heat source temperature changes from 120-130 °C. The mass-flow rate of R245fa is the main parameter adjusted by manually in the experiment. The steady and dynamic of parameters will be analyzed, and the optimal mass-flow rate of R245fa will be obtained from the experiment. The performances of the flash-binary power system are calculated by test data. Thermal properties of R245fa have obtained from NIST (Refprop 9.1) software. The main test data include the inlet and outlet pressure of expander P_5 and P_6, the inlet and outlet temperature of expander T_5 and T_6, R245fa mass-flow rate $\dot{m}_8$, hot water mass-flow rate $\dot{m}_9$, separator water mass-flow rate $\dot{m}_{s2}$, separator pressure P_{11}, separator temperature T_{11}, and rejection temperature T_{s5}. The performance indexes include First law efficiency, effective exergy efficiency and power output of per ton geofluid.

Hot water mass-flow rate is $\dot{m}_9$ and tested by turbine flowmeter:

$$\dot{m}_9 = \dot{m}_{10} \tag{1}$$

The vapor mass-flow rate of the flash system is m_{11} :

$$\dot{m}_{11} = \dot{m}_{10} - \dot{m}_{s2} \tag{2}$$

The specific exergy and exergy of state 9 are e_9 and Ex_9, respectively:

$$e_9 = h_9 - h_0 - T_0(s_9 - s_0) \tag{3}$$

$$Ex_9 = \dot{m}_9 e_9 \tag{4}$$

Power output of flash power subsystem:

$$w_{\text{F,turbine}} = \dot{m}_{11}(h_{11} - h_{12}) \tag{5}$$

Power output of binary power subsystem:

$$w_{\text{B,turbine}} = \dot{m}_8(h_5 - h_6) \tag{6}$$

Power output of flash-binary power system:

$$w_{\text{total}} = w_{\text{F,turbine}} + w_{\text{B,turbine}} \tag{7}$$

The isentropic efficiency of expender:

$$\eta_{\text{turbine}} = \frac{h_5 - h_6}{h_5 - h_{6\text{s}}} \tag{8}$$

Power output of per ton geofluid:

$$Ne = \frac{w_{\text{total}}}{3.6\dot{m}_9} \tag{9}$$

First efficiency of the flash-binary system:

$$\eta_1 = \frac{w_{\text{total}}}{\dot{m}_9(h_9 - h_{\text{s5}})} \tag{10}$$

The exergy efficiency is calculated based on a constant reference temperature:

$$\eta_2 = \frac{w_{\text{total}}}{Ex_9} \tag{11}$$

The uncertainty of directly measured parameters such as the temperature, the pressure and the flow rates are provided by the manufacturers, as shown in tab. 2. Uncertainties associated with each of the derived quantities such as power output, thermal efficiency and exergy efficiency are estimated by using the law of propagation of uncertainty. The uncertainty of derived quantity Y can be calculated:

$$U_{\text{y}} = \left[\left(\frac{\partial y}{\partial x_1}Ux_1\right)^2 + \left(\frac{\partial y}{\partial x_2}Ux_2\right)^2 + \ldots + \left(\frac{\partial y}{\partial x_{\text{n}}}Ux_{\text{n}}\right)^2\right]^{1/2} \tag{12}$$

where U_{x1}, U_{x2}, ..., U_{xn} are the uncertainties of the directly measured parameters of x_1, x_2, ..., x_n, respectively. Each variable sensitivity associated with the calculation of Y represented by partial differential parameters as $\partial y/\partial x_1$, $\partial y/\partial_2$,..., $\partial y/\partial x_n$ [34].

The value of uncertainty calculated for flash power subsystem capacity is ±3.2%, binary power subsystem capacity is ±2.8%, flash-binary power system capacity is ±3.1%, modified expander isentropic efficiency is ±4.5%, power output of per ton geofluid is ±3.2%, first-law efficiency is ±3.7% and effective exergy efficiency is ±3.8%.

Table. 2 Measured parameters and details of uncertainties

Measured parameter	Operation range	Accuracy	Model	Manufacturer
Temperature	0-200 °C	±0.1%	YH-WZP	Beijing Yuhang instrument group
Pressure	0-20 bar	±0.2%	YH202B	Beijing Yuhang instrument group
R245fa mass-flow rate	0-800 kg/h	±0.2%	YH-DMF13B	Beijing Yuhang instrument group
Hot water mass-flow rate	0.6-6 m^3/h	±0.1%	YH-LWD15SHB	Beijing Yuhang instrument group
Cooling watermass-flow rate	2-20 m^3/h	±0.1%	YH-LWD40SLB	Beijing Yuhang instrument group

Table. 3 Typical experimental operation data

	T_9 = 120 °C			T_9 = 130 °C		
States point	P [bar]	T [°C]	$\dot{m}$ [kgs^{-1}]	P [bar]	T [°C]	$\dot{m}$ [kgs^{-1}]
1	8.90	34.0	0.075	7.10	34.0	0.058
2	8.90	–	0.075	7.10	–	0.058
3	8.90	–	0.075	7.10	–	0.058
4	8.90	84.0	0.075	7.10	82.8	0.058
5	8.90	84.7	0.075	7.1	82.8	0.058
6	1.90	65.6	0.075	1.62	65.4	0.058
7	1.90	34.0	0.075	1.62	34.0	0.058
8	1.90	34.0	0.075	1.62	34.0	0.058
9	–	120.0	0.538	–	130	0.141
10	0.84	96.8	0.538	0.79	94.5	0.141
11	0.84	96.8	0.01	0.79	94.5	0.03
12	–	-	0.011	–	–	0.03
13	–	35.0	0.011	–	28.0	0.03
s1	–	96.8	0.527	–	94.5	0.138
s2	–	96.8	0.527	–	94.5	0.138
s3	–	-	0.527	–	–	0.138
s4	–	-	0.527	–	–	0.138
s5	–	86.5	0.527	–	75.8	0.138
c1		24.9	2.44		20.1	2.44
c2		–	1		-	1
c3		29.1	1		23	1
c4		–	1.44		–	1.44
c5		30.9	1.44		24	1.44

Results and discussion

In the experiment, the fraction of the shut-off valve in the flash system is 1/6, the mass-flow rate of R245fa is adjusted manually. The typical experiment operation data at 120 °C and 130 °C are shown in tab. 3. The environment temperature is 15 °C.

Experimental data analysis

Figure 4 gives the operational data of pressure and temperature at the condition of T_9 = 120 °C and T_9 = 130 °C, respectively. The left and right Y-axis represent mass-flow rate of R245fa ($\dot{m}_8$, black) and pressure/temperature values, respectively. The value of x-axis represents the experimental operation time. The mass-flow rate percentage of R245fa diaphragm pump increases from 16-35% at the heat source temperature is 120 °C. The P_5 (blue) increases with increasing $\dot{m}_8$ and fluctuates in 8.6 bar when the percentage is more than 26%. The P_6 (red) and P_{11} (green) maintain at 1.9 bar and 0.8, respectively. The T_{s2} (blue), T_{s5} (red), and T_5 (green) are about 97 °C, 86 °C, and 85 °C, respectively. When the percentage more than 26%, T_6 (purple) decreases sharply and the LED light of binary power subsystem flickers frequently. The optimal mass-flow rate of $\dot{m}_8$ is about 0.075 kg/s at 26% of the diaphragm pump.

The mass-flow rate percentage of R245fa diaphragm pump increases from 16-4% at the heat source temperature is 130 °C. The percentage of R245fa diaphragm pump cannot

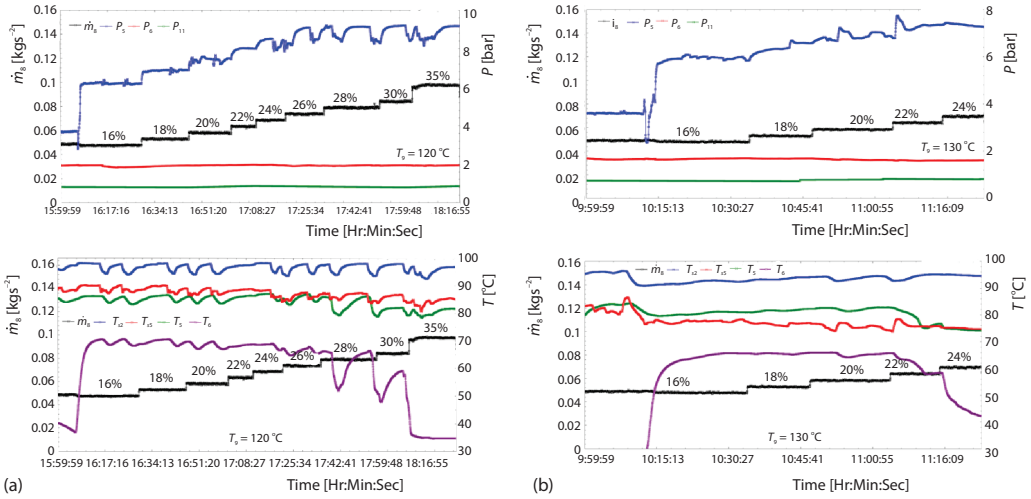

Figure 4. Pressure and temperature variation with time at T_9 = 120 °C and T_9 = 130 °C; (a) T_9 = 120 °C, (b) T_9 = 130 °C

be adjusted too much because of the power of heat source boiler. The P_5 (blue) increases with increasing $\dot{m}_8$ and fluctuates in 7.1 bar when the percentage is more than 20%. The P_6 (red) and P_{11} (green) maintain at 1.6 bar and 0.8 bar, respectively. The T_{s2} (blue), T_{s5} (red), and T_5 (green) are about 95 °C, 75.8 °C, and 83 °C, respectively. When the percentage is more than 20%, the T_6 (purple) decreases sharply from 66 °C and the LED light of binary power subsystem is flickering. The optimal mass-flow rate of $\dot{m}_8$ is about 0.058 kg/s at 20% of the diaphragm pump.

Figure 5 gives the operation data of mass-flow rate and cooling temperature at the condition of T_9 = 120 °C and T_9 = 130 °C, respectively. The left and right *Y*-axis represent mass-flow rate of R245fa ($\dot{m}_8$, black) and water mass-flow rate/cooling temperature, respectively. The value of *x*-axis represents the experimental operation time. The mass-flow rate percentage of R245fa diaphragm pump increases from 16% to 35% at the heat source temperature is 120 °C. The $\dot{m}_{10}$ (red) and $\dot{m}_{s2}$ (blue) fluctuate periodically when the percentage is less than 26%.

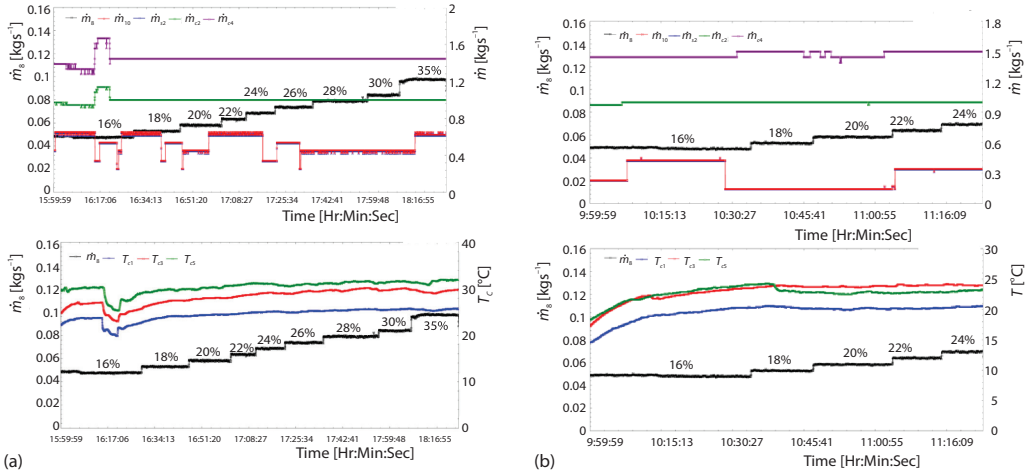

Figure 5. Mass-flow rate and cooling temperature variation with time at (a) T_9 = 120 °C and (b) T_9 = 130 °C

The $\dot{m}_{10}$ and $\dot{m}_{s2}$ are 0.54 kg/s and 0.53 kg/s, respectively, when the percentage is 26%. The $\dot{m}_{c2}$ (green), $\dot{m}_{c4}$ (purple), T_{c1} (blue), T_{c3} (red) and T_{c5} (green) are 1 kg/s, 1.44 kg/s, 25 °C, 29 °C and 31 °C, respectively.

The mass-flow rate percentage of R245fa diaphragm pump increases from 16-24% at the heat source temperature is 130 °C. The $\dot{m}_{10}$ and $\dot{m}_{s2}$ are 0.141 kg/s and 0.138kg/s, respectively, when the percentage is 20%. The $\dot{m}_{c2}$, $\dot{m}_{c4}$, T_{c1}, T_{c3}, and T_{c5} are 1 kg/s, 1.44 kg/s, 20 °C, 23 °C, and 24 °C, respectively.

The trend of operation parameters in fig. 5 corresponds to the parameters characteristics of fig. 4. The optimal mass-flow rate of $\dot{m}_8$ is about 0.075 kg/s at 26% of diaphragm pump and 0.058 kg/s at 20% of diaphragm pump, respectively when the heat source temperature is 120 ° C and 130 °C.

Performance evaluation

Figure 6 gives the output power of flash-binary system and subsystem. The left *Y*-axis represents mass-flow rate of R245fa ($\dot{m}_8$, black). The right *Y*-axis represents output power of flash-binary system (green), flash subsystem (red) and binary subsystem (blue), respectively. The value of *x*-axis represents the experimental operation time. The w_{total} (green), $w_{F,turbine}$ (red) and $w_{B,turbine}$ (blue) are calculated from the test values. The w_{total}, $w_{F,turbine}$, and $w_{B,turbine}$ are 1.5 kW, 1.1 kW, and 0.4 kW, respectively, at the condition of T_9 =120 °C and $\dot{m}_8$ = 0.075 kg/s, $w_{F,turbine}$ is nearly 3 times than $w_{B,turbine}$ at T_9 = 120 °C. The w_{total}, $w_{F,turbine}$, and $w_{B,turbine}$ are 0.67 kW, 0.32 kW, and 0.35 kW, respectively, at the condition of T_9 = 130 °C and $\dot{m}_8$ = 0.058 kg/s, $w_{F,turbine}$ is less than $w_{B,turbine}$ at T_9 = 130 °C. It can be seen that flash and binary power subsystem dominate the flash-binary power system at T_9 = 120 °C and T_9 = 130 °C, respectively. The higher heat source temperature is, the better for binary power subsystem. It should be given priority to the high capacity of binary power subsystem during design section when the heat source temperature is more than 130 °C.

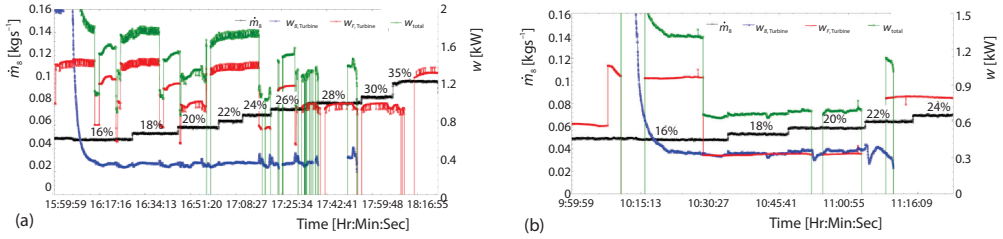

Figure 6. Power output performance with time at (a)T_9 = 120 °C and (b) T_9 = 130 °C

The isotropic efficiency of modified expender is calculated by test values. Figure 7 gives expander isotropic efficiency trend with increasing $\dot{m}_8$. The $\eta_{turbine}$ (blue) decreases sharply at the beginning of system operation and then fluctuates between 0.2 and 0.25 at the condition of T_9 = 120 °C or T_9 = 130 °C. The isotropic efficiency of a modified expander in binary power subsystem is just between 0.2 and 0.25 when flash-binary power system operates stably.

Power output per ton of geofluid is an important performance for the geothermal power plant. Figure 8 gives the power output trend among the flash-binary system operation. Power out per ton geogluid, *Ne,* (red) decreases firstly and then increases with increasing $\dot{m}_8$ (black), the system has an optimal mass-flow rate of R245fa when *Ne* reaches the stable value. The *Ne* is 0.78 kWh/t and 1.31 kWh/t, respectively at the condition of T_9 = 120 °C or T_9 = 130 °C when the system operates stably. The higher heat source temperature is, the higher power output.

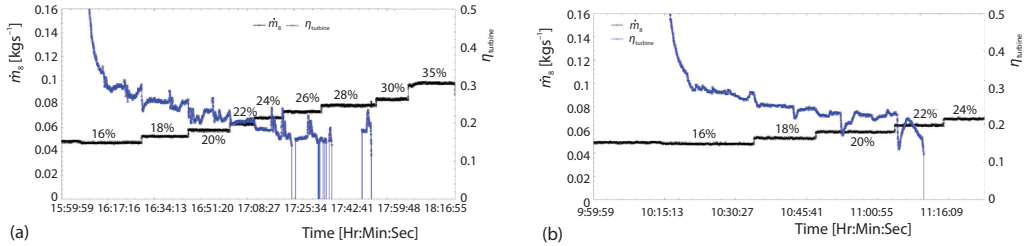

Figure 7. The isotropic efficiency of modified expender with time at (a) T_9 = 120 °C and (b) T_9 = 130 °C

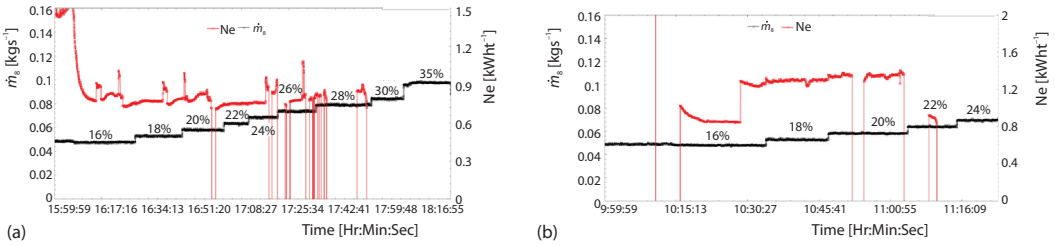

Figure 8. Power output per ton of geofluid with time at (a) T_9 = 120 °C and (b) T_9 = 130 °C

The flash-binary power system was also estimated by first law efficiency and exergy efficiency with respect to time as shown in fig. 9. The first law efficiency (blue) and exergy efficiency are 2.1% and 4.3%, respectively, when the system operates stably with T_9 = 120 °C. Correspondingly, these two values are 2.2% and 6.2%, respectively with T_9 = 130 °C. The low efficiency of the system is caused by the low efficiency of expender in power subsystem.

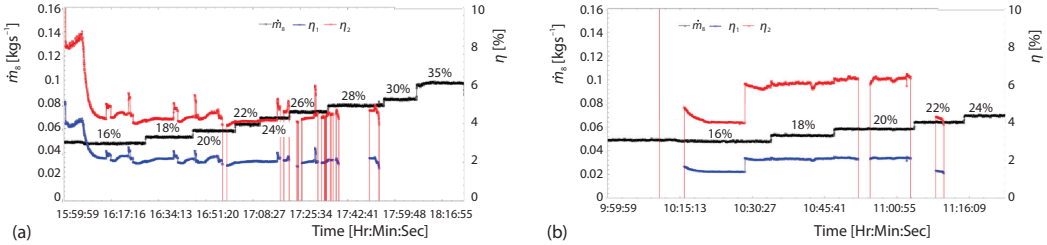

Figure 9. Efficiency performance with time at (a) T_9 = 120 ° C and (b) T_9 = 130 °C

Conclusions

A combined flash-binary experimental prototype of geothermal power generation system is newly established. Some valuable data obtained and applied in the future power plant construction from the experiment as.

- Flash and binary power subsystem dominate the flash-binary power system, respectively, when the heat source temperature are 120 °C and 130 °C. The efficiency of binary power subsystem should be priority during design section when the heat source temperature is higher than 130 °C.

- The power output of per ton geofluid are 0.78 kWh/t and 1.31 kWh/t, respectively, and when the heat source temperature are 120 ℃ and 130℃. The higher heat source temperature is, the better performance of flash-binary power system.
- The exergy efficiencies are 4.3% and 6.2%, respectively, with T_9 = 120 °C and T_9 = 130 °C because of the low efficiency of expander.

Acknowledgment

This work is sponsored by National Natural Science Funds (Grant No. 51406212).

Nomenclature

Ex – exergy, [kW]
e – specific exergy, [kJkg^{-1}]
$\dot{m}$ – mass-flow rate, [kgs^{-1}]
$w_{B,turbine}$ – power output of binary power subsystem, [kW]
$w_{F,turbine}$ – power output of flash power subsystem, [kW]
w_{total} – power output of flash-binary power system, [kW]
Ne – power out per ton geofluid, [kWht^{-1}]
P – pressure, [bar]
T – temperature, [°C]

Greek symbols

η_1 – first law efficiency of flash-binary system, [%]
η_2 – exergy efficiency, [%]
$\eta_{turbine}$ – isentropic efficiency of expender, [%]

Subscripts

1-8 – working fluid state
9-13 – hot water state
s1-s5 – separator water state
c1-c5 – cooling water state

References

[1] Hussain, A., *et al*., Emerging Renewable and Sustainable Energy Technologies, State of the Art, *Renewable and Sustainable Energy Reviews*, *71* (2017), May, pp.12-28
[2] DiPippo, R., *Geothermal Power Generation: Developments and Innovation*, Woodhead Publishing, Sawston, UK, 2016
[3] Bertani, R., Geothermal Power Generation in the World 2010-2014 Update Report, *Proceedings*, World Geothermal Congress 2015, Melbourne, Australia, 2015
[4] Wang, Y. Z., *et al.*, Multi-Objective Optimization and Grey Relational Analysis on Configurations of Organic Rankine Cycle, *Applied Thermal Engineering*, *114* (2017), Mar., pp. 1355-1363
[5] Bonalumi, D., Bombarda, P. C., Potential Performance of Environmental Friendly Application of ORC and Flash Technology in Geothermal Power Plants, *Energy Procedia*, *129* (2017), Sept., pp. 621-628
[6] Fallah, M., *et al*., A Comprehensive Comparison among Different Types of Geothermal Plants from Exergy and Thermoeconomic Points of View, *Thermal Science and Engineering Progress*, *5* (2018), Mar., pp.15-24
[7] Ozcan, N. Y., Gokcen, G., Thermodynamic Assessment of Gas Removal Systems for Single-Flash Geothermal Power Plants, *Applied Thermal Engineering*, *29* (2009), 14-15, pp. 3246-3253
[8] Jalilinasrabady, S., *et al*., Flash Cycle Optimization of Sabalan Geothermal Power Plant Employing Exergy Concept, *Geothermics*, *43* (2012), July, pp. 75-82
[9] Bina, S. M., *et al*., Exergoeconomic Analysis and Optimization of Single and Double Flash Cycles for Sabalan Geothermal Power Plant, *Geothermics*, *72* (2018), Mar., pp. 74-82
[10] Clarke, J., *et al*., The Constrained Design Space of Double-Flash Geothermal Power Plants Geothermics, *51* (2014), July, pp. 31-37
[11] Pambudi, N. A.. *et al.*, Performance Improvement of a Single-Flash Geothermal Power Plant in Dieng, Indonesia, upon Conversion a Double-Flash System Using Thermodynamic Analysis, *Renewable Energy*, *80* (2015), Aug., pp. 424-431
[12] Bao, J., Zhao, L., A Review of Working Fluid and Expander Selections for Organic Rankine Cycle, *Renewable and Sustainable Energy Reviews*, *24* (2013), Aug., pp. 325-343
[13] Chen, H., *et al*., A Review of Thermodynamic Cycles and Working Fluids for the Conversion of Low-grade Heat, *Renewable and Sustainable Energy Reviews*, *14* (2010), 9, pp. 3059-3067
[14] Imran, M., Usman, M., Byung-Sik Park, Comparative Assessment of Organic Rankine Cycle Integration for Low Temperature Geothermal Heat Source Applications, *Energy*, *102* (2016), May, pp. 473-490

[15] Gao, P. L., *et al*., Experimental Investigation on a Small Pumpless ORC (Organic Rankine Cycle) System Driven by the Low Temperature Heat Source, *Energy*, *91* (2015), Nov., pp. 324-333
[16] Quoilin, S., *et al*., Dynamic Modelling and Optimal Control Strategy of Waste Heat Recovery Organic Rankine Cycles, *Applied Energy*, *88* (2011), 6, pp. 2183-2190
[17] Fu, B. R., *et al*., Effect of off-Design Heat Source Temperature on Heat Transfer Characteristics and System Performance of a 250-kW Organic Rankine Cycle System, *Applied Thermal Engineering*, *70* (2014), 1, pp. 7-12
[18] Pei, G., *et al*., Construction and Dynamic Test of a Small-Scale Organic Rankine Cycle, *Energy*, *36* (2011), 5, pp. 3215-3223
[19] Chang, J., *et al*., Experimental Study on Low-Temperature Organic Rankine Cycle Utilizing Scroll Type Expander, *Applied Energy, 155* (2015), Oct., pp. 150-159
[20] Dickes, R., *et al*., Modelling of Organic Rankine Cycle Power Systems in off-Design Conditions: An Experimentally-Validated Comparative Study, *Energy*, *123* (2017), Mar., pp. 710-727
[21] Li, L., *et al*., Experimental Investigations into Power Generation with Low Grade Waste Heat and R245fa Organic Rankine Cycles (ORC), *Applied Thermal Engineering*, *115* (2017), Mar., pp. 815-824
[22] Song, P., *et al*., A Review of Scroll Expanders for Organic Rankine Cycle Systems, *Applied Thermal* Engineering, *75* (2015), Jan., pp. 54-64
[23] Wu, Z., *et al*., Experimental Testing and Numerical Simulation of Scroll Expander in a Small Scale Organic Rankine Cycle System, *Applied Thermal Engineering*, *87* (2015), Aug., pp. 529-537
[24] Chang, J. C., *et al*., Experimental Study and CFD Approach for Scroll Type Expander Used in Low-Temperature Organic Rankine Cycle, *Applied Thermal Engineering*, *73* (2014), 2, pp. 1444-1452
[25] Bracco, R., *et al*., Experimental Tests and Modelization of a Domesticscale ORC (Organic Rankine Cycle, Energy, *58* (2013), Sept., pp. 107-116
[26] Quoilin, S., *et al*., Experimental Study and Modelling of an Organic Rankine Cycle Using Scroll Expander, *Applied Energy*, *87* (2010), 4, pp. 1260-1268
[27] Twomey, B., *et al*., Dynamic Performance Estimation of Small-Scale Solar Cogeneration with an Organic Rankine Cycle Using a Scroll Expander, *Applied Thermal Engineering*, *51* (2013), 1-2, pp. 1307-1316
[28] Liu, G., *et al*., Theoretical and Experimental Research on Scroll Expander Used in Small-Scale Organic Rankine Cycle System, *Journal of Process Mechanical Engineering*, *229* (2015), 1, pp. 25-35
[29] Zeyghami, M., Performance Analysis and Binary Working Fluid Selection of Combined Flash-Binary Geothermal Cycle, *Energy*, *88* (2015), Aug., pp. 765-774
[30] Wang, J. Y., *et al*., Thermodynamic Analysis and Optimization of a Flash-Binary Geothermal Power Generation System, *Geothermics*, *55* (2015), May, pp. 69-77
[31] Yilmaz, C., *et al*., Exergetic Cost Evaluation of Hydrogen Production Powered by Combined Flash-Binary Geothermal Power Plant, *International Journal of Hydrogen Energy, 40* (2015), 40, pp. 14021-14030
[32] Aali, A., *et al*., Exergoeconomic Analysis and Multi-Objective Optimization of a Novel Combined Flash-Binary Cycle for Sabalan Geothermal Power Plant in Iran, *Energy Conversion and Management*, *143* (2017), July, pp. 377-390
[33] Zhao, Y. Wang, J., Exergoeconomic Analysis and Optimization of a Flash-Binary Geothermal Power System , *Applied Energy*, *179* (2016), Oct., pp. 159-170
[34] Moffat, R. J., Describing the Uncertainties in Experimental Results, *Experimental Thermal and Fluid Science*, *1* (1988), 1, pp. 3-17

Paper submitted: November 12, 2018
Paper revised: December 25, 2018
Paper accepted: December 26, 2018